
Releasing Inequality Phenomena in L_∞ -Adversarial Training via Input Gradient Distillation

Junxi Chen *

chenjx353@mail2.sysu.edu.cn

Junhao Dong *

dongjh8@mail2.sysu.edu.cn

Xiaohua Xie *

xiexiaoh6@mail.sysu.edu.cn

Abstract

Since adversarial examples appeared and showed the catastrophic degradation they brought to DNN, many adversarial defense methods have been devised, among which adversarial training is considered the most effective. However, a recent work showed the inequality phenomena in l_∞ -adversarial training and revealed that the l_∞ -adversarially trained model is vulnerable when a few important pixels are perturbed by i.i.d. noise or occluded. In this paper, we propose a simple yet effective method called Input Gradient Distillation to release the inequality phenomena in l_∞ -adversarial training. Experiments show that while preserving the model's adversarial robustness, Input Gradient Distillation improves the model's robustness to i.i.d. noise and occlusion. Moreover, we formally explain why the equality of the model's saliency map can improve the model's robustness to i.i.d. noise or occlusion.

1 Introduction

In 2013, Szegedy et al. [1] discovered adversarial examples, which can fool DNN by adding an imperceptible perturbation to a clean sample, and raised public concerns about DNN's security and reliability. Since then, many adversarial defense methods, including adversarial training[1–3], adversarial example detection[4, 5], etc., have been proposed to improve DNN's robustness to adversarial examples, among which adversarial training is considered the most effective.

Besides improving DNN's adversarial robustness, another advantage that adversarial training has is found. Chalasani et al. [6] showed that l_∞ -adversarial training tends to produce sparse and stable Integrated Gradients-based[7] attribution tensors. They think such sparseness means producing a concise explanation, where only the input features with significant contributions are included. In a word, the suppression of non-robust or non-significant features is considered a benefit that adversarial training brings.

However, a recent study showed that such suppression will result in unrealized threats. Duan et al. [8] found the inequality phenomena on the input attribution map that occur during the l_∞ -adversarial training and these phenomena make the model less reliable. To be specific, they showed that the l_∞ -adversarially trained model produces attribution maps with higher Gini value[9] compared to the standard-trained model and is more vulnerable than the standard-trained model when a few pixels with high attribution values are perturbed by i.i.d. noise or are occluded.

*The authors are with the School of Computer Science and Engineering, Sun Yat-sen University, 510006, Guangzhou, China, and with the Guangdong Province Key Laboratory of Information Security Technology, 510006, Guangzhou, China, and also with and the Key Laboratory of Machine Intelligence and Advanced Computing, Ministry of Education, 510006, Guangzhou, China.

In this paper, we utilize the standard-trained model’s input gradients as guidance to release inequality phenomena in the l_∞ -adversarially trained model. The method is called "Input Gradient Distillation", or IGD for short. Also, a formalized analysis of the relationship between the Gini value of the model’s saliency map and the model’s robustness to i.i.d. noise and occlusion is conducted. Experiment results show that IGD can dramatically release the inequality phenomena in l_∞ -adversarial training and improve the l_∞ -adversarially trained model’s robustness to attacks devised by Duan et al. [8] while preserving the adversarial robustness of the l_∞ -adversarially trained model. Specifically, attacked by inductive noise, IGD decreases l_∞ -adversarially trained model’s error rate from around 70% to around 10% on Imagenet-100. After training with IGD, the error rate of the model attacked by inductive occlusion drops from around 40.76% to 24.23% on Imagenet-100, and the IGD-trained model generalizes well to different occlusion colors compared to CutOut used by Duan et al. [8]. We also test our method on noisy images of Imagenet-C[10]. Results show that IGD-trained models have better robustness to Gaussian noise, impulse noise, and shot noise compared to the PGDAT-trained model with up to 21.11% descent in the error rate.

Main contributions of our paper are as follows:

- We propose a method, called "Input Gradient Distillation"(IGD for short), to release the inequality phenomena in l_∞ -adversarial training. Experiments show that the model trained with IGD tends to have a more equal attribution map and better robustness to i.i.d. noise and occlusion compared to the PGDAT-trained model while preserving adversarial robustness.
- We formally analyze the relationship between the Gini value(a metric to evaluate inequality) of saliency maps and models’ robustness to noise and occlusion. Theoretical analysis proves that a more equal saliency map leads to a smaller deviation in class score brought by input space noise or occlusion. We also explain why such robustness improvement is not notable on low-resolution datasets like CIFAR100.

2 Related Works

In this section, we introduce works related to this paper. In subsection 2.1, we introduce the concept of l_∞ -adversarial training. In subsection 2.2, we introduce works that utilized input gradient for adversarial defense. In subsection 2.3, we explain how the inequality phenomena in l_∞ -adversarial training are defined and measured. In subsection 2.4, we introduce attack algorithms devised by Duan et al. [8].

2.1 L_∞ -adversarial training

The main idea of adversarial training is adding adversarial examples in the training phase. Madry et al. [2] improved DNN’s adversarial robustness by solving a min-max optimization problem:

$$\min_{\theta} \max_{\delta} L(f_{\theta}(x + \delta), y), s.t. \|\delta\|_p \leq \epsilon \tag{1}$$

where the inner maximum problem can be solved by PGD algorithm[2]. If we define $p = \infty$, then the training is called l_∞ -adversarial training. In this paper, we only use PGD to solve the inner maximum problem and set $p = \infty$.

2.2 Using input gradients for adversarial defense

Using input gradients for adversarial defense is not a completely new idea. Previous works [11, 12] have attempted to improve DNN’s adversarial robustness by penalizing the L_2 norm of input gradients. Other works, such as [13–15], aimed to align the input gradient of the model being trained with some external guidance in order to obtain or enhance adversarial robustness. The studies mentioned above demonstrate that incorporating input gradients into the loss function can effectively enhance the model performance.

2.3 Inequality phenomena in L_∞ -adversarial training

As mentioned in section 1, Duan et al. [8] found that compared to standard training, l_∞ -adversarial training will make DNN produce a more unequal input attribution map(For brevity, we use $A^f(x)$,

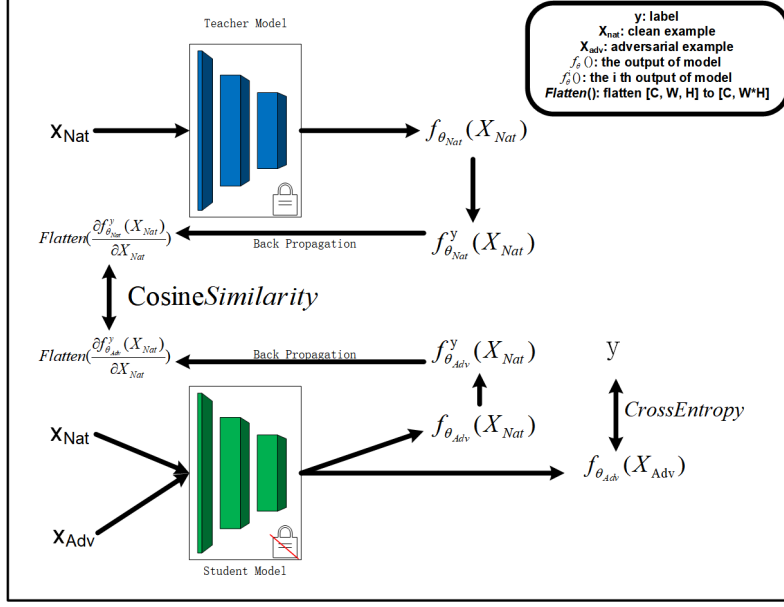


Figure 1: The framework of IDG.

where f stands for DNN and x stands for input). They used Gini value[9] to evaluate such inequality phenomena, formally:

$$Gini(\Phi) = \frac{1}{n} * (n + 1 - 2 * \frac{\sum_{i=1}^n (n + 1 - i) * \phi_i}{\sum_{i=1}^n \phi_i}) \quad (2)$$

where $\Phi = \{\phi_i, i = 1 \dots n \mid \phi_i \leq \phi_{i+1}\}$. The higher the Gini value is, the more unequal the Φ is.

Duan et al. [8] defined two types of inequality: Global inequality and regional inequality. These two types of inequality are both measured by the Gini value. For global inequality, they calculate the Gini value of $A^f(x)$ ($Gini(A^f(x))$ for short). For regional inequality, they first divide $A^f(x)$ into blocks with size $r \times r$ and sum up values within the block to get a downsampled attribution map ($A_r^f(x)$ for short). Then, they calculate the Gini value of $A_r^f(x)$ ($Gini(A_r^f(x))$ for short).

2.4 Attacks devised for the inequality phenomena

To reveal threats brought by the inequality phenomena, Duan et al. [8] devised two attack algorithms to attack l_∞ -adversarially trained models, called Inductive noise attack and Inductive occlusion attack.

2.4.1 Inductive Noise Attack

Inductive noise attack (INA for short) uses $A^f(x)$ as guidance to perturb samples with Gaussian noise $\sigma \in \mathcal{N}(0, 1)$ in an order determined by the importance of pixels (features). Formally, we have:

$$x' = x + M * \sigma, \text{ where } M = \begin{cases} 1, & a_i > \text{threshold} \\ 0, & a_i \leq \text{threshold} \end{cases} \text{ and } a_i \in A^f(x). \text{ Besides the additive noise}$$

introduced above, Duan et al. [8] also devised an attack in which the original pixel is replaced by noise. Formally, we have $x' = \bar{M} * x + M * \sigma$, where $\bar{M} = 1 - M$. For conciseness, we refer to the former INA as "INA1" and to the latter INA as "INA2".

2.4.2 Inductive Occlusion Attack

Inductive occlusion attack (IOA) gradually occludes regions with high attribution values. In each iteration, IOA selects the n biggest pixels as regions' central points and occludes regions with $(2r + 1) \times (2r + 1)$ pure color. Duan et al. [8] set N and R to limit n and r , and chose black, gray,

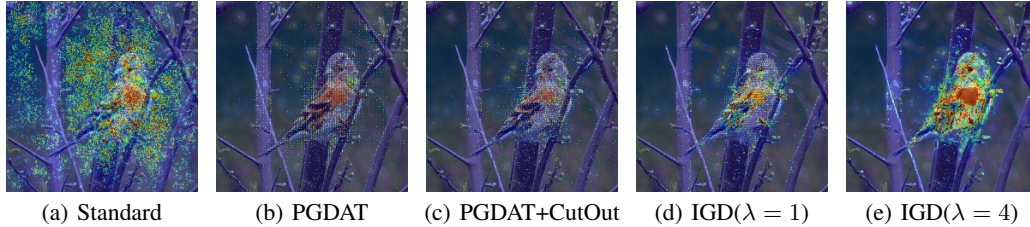


Figure 2: Visualizations of feature attribution maps of Imagenet-100.

and white colors to occlude the image. For simplicity, we refer to IOA with black, gray, and white occlusion colors as IOA-B, IOA-G, and IOA-W, respectively.

Besides two inductive methods mentioned above, Duan et al. [8] also used random noise(RN for short) to attack DNN, which randomly selects several pixels and perturbs them with Gaussian noise $\sigma \in \mathcal{N}(0, 1)$.

3 Methodology

Now we introduce our approach, Input Gradient Distillation, which can release the inequality phenomena in l_∞ -adversarial training. The main idea of IGD is to force the l_∞ -adversarially trained model to have attribution maps similar to the standard-trained model’s. The overall framework is shown in Figure 1. During the l_∞ -adversarial training, we feed clean inputs into a fixed standard-trained model and our target model, and align their input gradients.

As for the choice of the distance metric, our goal is not to change the absolute value of the gradient, but to change the relative value, as we don’t want to alter the model’s adversarial robustness and [11, 12] claimed that the norm of the input gradient has a strong correlation with adversarial robustness. Thus, when viewing a 2-D attribution map as a 1-D attribution vector, we align the direction of the attribution vector by using cosine similarity because we have $Gini(k * \phi) = Gini(\phi)$ and $cosine_similarity(k * \vec{v}, \vec{v}) = 1$, where $k * \phi = \{k * \phi_i, i = 1 \dots n \mid \phi_i \leq \phi_{i+1}\}$. Formally, we have our loss function:

$$Loss = CE(y, f_{\theta_{Adv}}(x')) - \lambda * \cos(Flatten(\frac{\partial f_{\theta_{Adv}}^y(x)}{\partial x}), Flatten(\frac{\partial f_{\theta_{Std}}^y(x)}{\partial x})) \quad (3)$$

where x' is a adversarial example, λ is a coefficient. The first item of Equation 3 is the same as the loss proposed by Madry et al. [2]. By optimizing the second item of Equation 3, we force the l_∞ -adversarially trained model’s input gradient to be close to the standard-trained model’s.

4 Experiments

In this section, we will introduce the details of our experiment and analyze the performance of Input Gradient Distillation(IGD). In subsection 4.1, we will show that IGD can release the inequality phenomena in l_∞ -adversarial training and visualize attribution maps. In subsection 4.2 and subsection 4.3, we will show IGD-trained models’ robustness to INA and IOA introduced in subsection 2.4 and comparisons to other methods. In subsection 4.4, we compare models’ robustness to RN and noisy images of Imagenet-C. Our experiments are mainly conducted on CIFAR100[16] and Imagenet-100[17] using ResNet18[18]. We mainly use Saliency map to generate attribution maps, where $A^f(x) = \frac{\partial f^y(x)}{\partial x}$. The setup of our experiment is shown in subsection A.2.

4.1 Releasing the inequality phenomena

In this part, we show the effectiveness of IGD in releasing the inequality phenomena and comparisons to other methods. Table 1 shows that IGD can dramatically release the global inequality in l_∞ -adversarial training and control the level by tuning coefficient λ . On Imagenet-100, IGD can decrease PGDAT’s $Gini(A^f(x))$ by up to 26% and decrease PGDAT’s $Gini(A^f(x))$ by up to 9% on CIFAR100, while CutOut can only slightly release the global inequality by up to 1%. In Table 2,

Table 1: The standard accuracy, adversarial accuracy, global Gini value, and regional Gini value of Resnet18 across different datasets and methods.

Dataset	Method	Metric			
		Std. Acc. \uparrow	Adv. Acc. \uparrow	$Gini(A^f(x))$	$Gini(A_r^f(x))$
CIFAR100	Standard	77.56%	0.00%	0.530(80%)	0.342(65%)
	PGDAT [2]	57.62%	24.61%	0.666(100%)	0.527(100%)
	PGDAT+CutOut [8]	53.77%	23.62%	0.665(100%)	0.524(99%)
	IGD($\lambda=1$)	58.04%	24.83%	0.663(100%)	0.526(100%)
	IGD($\lambda=2$)	57.79%	24.33%	0.638(96%)	0.507(96%)
	IGD($\lambda=3$)	56.39%	23.45%	0.617(93%)	0.489(93%)
	IGD($\lambda=4$)	57.02%	22.43%	0.603(91%)	0.475(90%)
Imagenet-100	Standard	87.32%	0%	0.544(58%)	0.328(58%)
	PGDAT [2]	70.74%	33.28%	0.933(100%)	0.565(100%)
	PGDAT+CutOut [8]	70.36%	32.54%	0.924(99%)	0.558(99%)
	IGD($\lambda=1$)	71.42%	33.02%	0.834(89%)	0.557(99%)
	IGD($\lambda=2$)	71.92%	32.28%	0.737(79%)	0.554(98%)
	IGD($\lambda=3$)	72.10%	31.82%	0.705(76%)	0.536(95%)
	IGD($\lambda=4$)	72.18%	31.20%	0.694(74%)	0.532(94%)

Table 2: $\left\| \frac{\partial f^y(x)}{\partial x} \right\|_1$ of Resnet18 across different datasets and methods.

Dataset	Method	$\left\ \frac{\partial f^y(x)}{\partial x} \right\ _1$
CIFAR100	Standard	27563724(100%)
	PGDAT [2]	660362(2.40%)
	PGDAT+CutOut [8]	570716(2.07%)
	IGD($\lambda=1$)	652751(2.37%)
	IGD($\lambda=2$)	616606(2.24%)
	IGD($\lambda=3$)	573567(2.08%)
	IGD($\lambda=4$)	629620(2.28%)
Imagenet-100	Standard	22982087(100%)
	PGDAT [2]	446562(1.94%)
	PGDAT+CutOut [8]	455458(1.98%)
	IGD($\lambda=1$)	463524(2.02%)
	IGD($\lambda=2$)	466847(2.03%)
	IGD($\lambda=3$)	468178(2.04%)
	IGD($\lambda=4$)	460062(2.00%)

IGD doesn't change $\left\| \frac{\partial f^y(x)}{\partial x} \right\|_1$ a lot compared to the PGDAT-trained model, which accords with our assumption that IGD aligns the direction and has little influence on the norm of the saliency map. Though IGD can release global inequality well, it can not release regional inequality effectively. This means that pixels with a high attribution value tend to cluster in a few regions. We also report the Gini value of $A^f(x)$ and $A_r^f(x)$ generated by other four attribution methods in subsection A.10, where our findings in Table 1 still hold. As for preserving the model's adversarial robustness, the adversarial accuracy only drops 1-2% on Imagenet-100 and on CIFAR100. IGD can even slightly promote the model's standard accuracy on both Imagenet-100 and CIFAR100.

For a more intuitive explanation of how IGD works, we visualize attribution maps on Imagenet-100 in Figure 2. Pixels on visualized attribution maps with warm colors have high attribution values and actually dominate the prediction[8]. In Figure 2, warm color pixels in attribution maps of PGDAT are much fewer than Standard's and IGDs', which indicates IGD-trained models have a relatively equal decision pattern and explains IGD-trained models' lower $Gini(A^f(x))$. As for the PGDAT-trained model with CutOut, its attribution map does not have visual differences from the PGDAT-trained model, which is consistent with our findings in Table 1. We can also find that there are fewer warm color pixels on the background in IGDs' attribution maps than in standard's. The warm color pixels mainly lie on perceptually-aligned areas like bird wings. This explains IGD's relatively high $Gini(A_r^f(x))$: important pixels tend to cluster in a few regions. However, with large λ , the area of warm color pixels begins to grow, and $Gini(A_r^f(x))$ decreases. More visualizations are shown in subsection A.13.

To conclude, unlike PGDAT's focusing on "robust pixels", models trained with IGD tend to focus on "robust regions", which contain many important pixels. The equality within the robust region releases global inequality but may not be effective in releasing regional inequality. As a comparison, CutOut will force the model to find robust pixels in different regions. However, it can't release global inequality, because its prediction still relies on a few pixels.

4.2 Robustness to INA

In this part, we compare the INA-robustness of models trained with different methods. Results are shown in Figure 3(a), Figure 3(b), Figure 4(a), and Figure 4(b). On Imagenet-100, all dashed lines are far below the orange line, which indicates that IGD can effectively improve l_∞ -adversarially trained model's robustness to INA. When $\lambda > 1$, models trained with IGD even have better robustness to INA than the standard-trained model. On CIFAR100, both PGDAT- and IGD-trained models have better robustness to INA compared to the standard-trained model, but improvement of INA-robustness gained by IGD is minor, which we hypothesize is due to the resolution difference between datasets and the gap of $Gini(A^f(x))$ (see subsection 5.2). On CIFAR100 and Imagenet-100, all IGD- and PGDAT-trained models have a higher $Gini(A^f(x))$ than the standard-trained model, but some of them still have better robustness to INA. This indicates that a higher $Gini(A^f(x))$ does not necessarily indicate worse robustness to INA, which we will explain in detail in section 5. Error rates of models attacked by INA with different attribution methods are shown in subsection A.11.

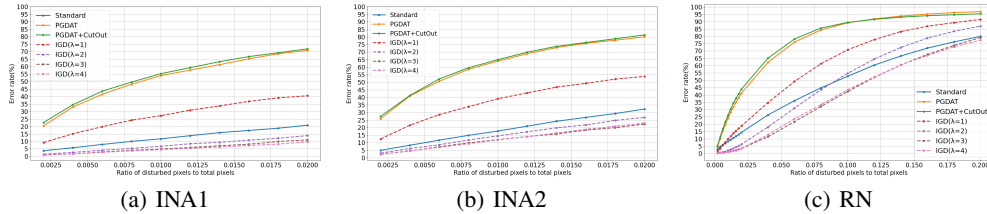


Figure 3: Error rate↓ of Resnet18 trained with different methods on Imagenet-100.

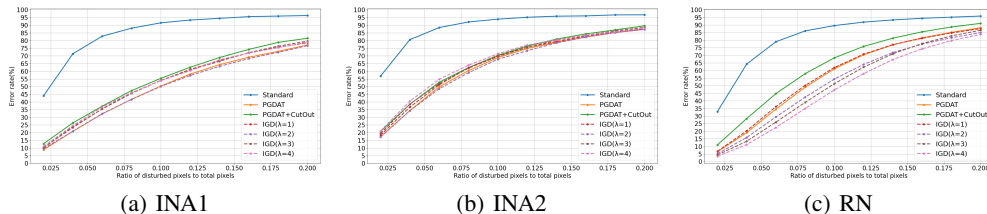


Figure 4: Error rate↓ of Resnet18 trained with different methods on CIFAR100.

4.3 Robustness to IOA

In this part, we compare the IOA-robustness of models trained with different methods. Results are shown in Table 3. On CIFAR100, both PGDAT- and IGD-trained models have better robustness to IOA than the standard-trained model and IGD slightly improves IOA-robustness compared to the PGDAT-trained model. On Imagenet-100, the PGDAT-trained model has worse IOA-robustness than the standard-trained, which is consistent with Duan et al. [8]’s conclusion. Because of IGD’s releasing the inequality phenomena, most of the models trained with IGD tend to have competitive robustness to IOA. When $\lambda=2$ to 4, IGD-trained models have better robustness to IOA-G and IOA-W compared to models trained with other methods. We also notice that with $\lambda = 1$, IGD only decreases error rates by up to 2% or even degrades IOA-robustness(see subsection A.12) compared to the PGDAT-trained model, which we will discuss in subsection 5.1. Another interesting finding is that IOA-robustness gained by IGD has better generalization than that gained by CutOut. The PGDAT-trained model using CutOut has competitive robustness to IOA-B but has similar or even worse robustness to IOA-G and IOA-W compared to the PGDAT-trained model. Error rates of models attacked by IOA with other attribution methods are shown in subsection A.12.

4.4 Robustness to i.i.d. random noise

Apart from inductive attacks introduced in subsection 2.4, we use RN to evaluate the robustness of models trained on CIFAR100 and Imagenet-100. We also use noisy images in the subset of Imagenet-C[10], which has the same classes as Imagnet-100, to evaluate the robustness of models trained on Imagenet-100. The main difference between noisy images of Imagenet-C and RN is that the variance of the random noise in Imagenet-C is smaller than RN. Results on RN are shown in Figure 3(c) and Figure 4(c). Results on noisy images of Imagenet-C are shown in Table 5, Table 6, and Table 7.

For RN, on Imagenet-100, we can find that though pixels attacked by i.i.d. noise are randomly selected, the PGDAT-trained model is still more vulnerable than the standard-trained model. Like results on INA, IGD can promote l_∞ -adversarially trained model’s robustness to RN. On CIFAR100, the improvement in RN-robustness brought by IGD is not as notable as that on Imagenet-100. As for results on Imagenet-C, We can see that all IGD-trained models have lower error rates compared to the standard-trained model and the PGDAT-trained model. IGD can reduce the error rate of models by up to 21.11% compared to the PGDAT-trained model. We also find that CutOut worsens the PGDAT-trained model’s robustness to noise, and increases the PGDAT-trained model’s error rate by up to 4.9%. Unlike results shown in subsection 4.2, the standard-trained model has worse robustness to noisy images in Imagenet-C than the PGDAT-trained model, which we will discuss in subsection 5.1.

Table 3: Error rate \downarrow of Resnet18 across different methods, datasets, and types of IOA.

Dataset	Attack			
	Method	IOA-B	IOA-G	IOA-W
CIFAR100	Standard	56.17%	36.11%	52.23%
	PGDAT [2]	40.48%	18.04%	40.91%
	PGDAT+CutOut Duan et al. [8]	12.56%	17.64%	40.53%
	IGD($\lambda=1$)	37.61%	16.48%	41.10%
	IGD($\lambda=2$)	37.08%	16.26%	38.94%
	IGD($\lambda=3$)	37.51%	16.90%	39.20%
	IGD($\lambda=4$)	38.56%	17.17%	39.06%
Imagenet-100	Standard	17.59%	8.25%	13.71%
	PGDAT [2]	32.31%	10.85%	40.76%
	PGDAT+CutOut [8]	21.17%	10.12%	39.94%
	IGD($\lambda=1$)	31.49%	10.22%	38.30%
	IGD($\lambda=2$)	22.68%	5.98%	28.53%
	IGD($\lambda=3$)	19.82%	5.19%	24.62%
	IGD($\lambda=4$)	18.01%	5.46%	24.23%

Table 4: Average $(\sum_{i=1}^k w_{d_i})^2$ and $\sum_{i=1}^k w_{d_i}^2$ of Resnet18 attacked by IOA, and average confidence of correctly classified sample across different methods on Imagenet-100.

Method	$\sum_{i=1}^k w_{d_i}^2$	$(\sum_{i=1}^k w_{d_i})^2$	Confidence
Standard	166.21	169.09	96.73%
PGDAT [2]	1.12	8.75	77.07%
PGDAT+CutOut [8]	1.06	9.53	77.43%
IGD($\lambda=1$)	0.76	9.44	78.60%
IGD($\lambda=2$)	0.3	7.12	79.29%
IGD($\lambda=3$)	0.24	6.04	79.29%
IGD($\lambda=4$)	0.21	5.73	78.50%

5 Discussion

5.1 Explanation of IGD- and standard-trained models' robustness to noise and occlusion

In this paper, we test two types of noise. One is the additive noise like Gaussian noise and Poisson noise, where $x' = x + \delta * m$, and the other is the multiplicative-additive noise like INA2 and impulse noise, where $x' = x * (1 - m) + \delta * m$. For conciseness, we also view occlusion as a kind of noise, whose formula of x' is the same as the multiplicative-additive noise's.

For simplicity, we first consider a linear score model $f(\vec{x}) = \vec{w}^T \vec{x} + b$ ($\vec{w}, \vec{x} \in R^{n \times 1}$, and $b \in R$) attacked by some i.i.d. additive noise $\vec{\delta} \in R^{n \times 1}$ ($\delta_i \sim \mathcal{D}(\mu_\delta, \sigma_\delta^2)$) that is masked by $\vec{m} \in \{0, 1\}^{n \times 1}$ having $\|\vec{m}\|_0 = k$. Formally, we have $y' = \vec{w}^T (\vec{x} + \vec{\delta} * \vec{m}) + b = y + \vec{w}^T (\vec{\delta} * \vec{m}) = y + y_\delta$, where $y_\delta \sim \mathcal{D}(\mu_\delta \sum_{i=1}^k w_{d_i}, \sigma_\delta^2 \sum_{i=1}^k w_{d_i}^2)$ ($d_i < d_{i+1}$ and $1 \leq d_i \leq n$), y is the clean sample's score, and \vec{w} can be viewed as model f 's saliency map[19].

For Gaussian noise and Poisson noise, we have $\mu_\delta = 0$ and $y_\delta \sim \mathcal{D}(0, \sigma_\delta^2 \sum_{i=1}^k w_{d_i}^2)$. We can suppress y_δ 's impact in two ways: one is enlarging y to submerge y_δ , and the other is directly suppressing y_δ . We mainly discuss the latter one. Because IGD does not significantly change clean samples' confidence (see Table 4) and $\left\| \frac{\partial f^y(x)}{\partial x} \right\|_1$ (see Table 2), we assume that y and $\|\vec{w} * \vec{m}\|_1$ are fixed. Thus, we suppress $E \{(y' - y)^2\} = \sigma_\delta^2 \sum_{i=1}^k w_{d_i}^2$ by solving:

$$\text{minimize } \sum_{i=1}^k w_{d_i}^2, \quad \text{s.t. } \sum_{i=1}^k |w_{d_i}| - C = 0$$

Using Lagrange Multiplier Method, we have $|w_{d_i}| = \frac{C}{k}$. This indicates that if the $\|\vec{w} * \vec{m}\|_1$ is fixed or kept on certain scale, then f has the best additive noise robustness when $\vec{w} * \vec{m}$ is totally equal, where $Gini(\vec{w} * \vec{m}) = 0$. Also, we have $\frac{C^2}{k} \leq \sum_{i=1}^k w_{d_i}^2 \leq C^2$, which means we can suppress the upper bound of the deviation of class score by decreasing $\|\vec{w} * \vec{m}\|_1$.

Some may question that when $\|\vec{w} * \vec{m}\|_1$ is fixed, does decreasing $Gini(\vec{w} * \vec{m})$ means decreasing y_σ 's standard deviation? For two non-zero elements in $\vec{w} * \vec{m}$, saying w_a and w_b , where $|w_a| < |w_b|$, the only way to decrease $Gini(\vec{w} * \vec{m})$ is to increase $|w_a|$ by Δ and decrease $|w_b|$ by Δ , where $|w_b| - |w_a| \geq 2 * \Delta$. This can be gradually achieved without changing elements' relative positions

Table 5: Error rate \downarrow on Imagenet-C's Gaussian noise.

Model	Severity				
	1	2	3	4	5
Standard	15.19%	35.50%	66.31%	88.23%	96.45%
PGDAT[2]	5.06%	14.07%	38.17%	69.43%	91.98%
PGDAT+CutOut[8]	4.54%	14.73%	42.37%	74.33%	93.26%
IGD($\lambda=1$)	3.02%	10.06%	28.47%	60.32%	88.79%
IGD($\lambda=2$)	3.42%	9.30%	26.07%	56.67%	86.92%
IGD($\lambda=3$)	2.86%	8.25%	24.03%	52.93%	85.44%
IGD($\lambda=4$)	3.62%	9.50%	23.64%	51.31%	82.74%

Table 6: Error rate \downarrow on Imagenet-C's impulse noise.

Model	Severity				
	1	2	3	4	5
Standard	34.45%	57.53%	72.65%	90.60%	96.09%
PGDAT [2]	13.77%	33.43%	53.19%	81.20%	94.61%
PGDAT+CutOut[8]	14.73%	37.84%	56.71%	84.62%	95.00%
IGD($\lambda=1$)	9.99%	24.95%	40.86%	73.60%	91.35%
IGD($\lambda=2$)	7.69%	21.83%	37.57%	69.79%	90.43%
IGD($\lambda=3$)	6.21%	18.34%	32.08%	65.38%	88.82%
IGD($\lambda=4$)	7.50%	19.76%	32.71%	63.25%	85.93%

Table 7: Error rate \downarrow on Imagenet-C's shot noise.

Model	Severity				
	1	2	3	4	5
Standard	18.28%	39.78%	65.78%	88.53%	94.25%
PGDAT[2]	7.65%	20.68%	45.13%	77.22%	90.11%
PGDAT+CutOut[8]	6.96%	21.79%	49.05%	81.33%	91.72%
IGD($\lambda=1$)	4.80%	14.83%	33.89%	70.02%	86.16%
IGD($\lambda=2$)	4.67%	14.07%	31.20%	66.47%	83.83%
IGD($\lambda=3$)	3.91%	12.36%	29.36%	65.15%	83.73%
IGD($\lambda=4$)	4.34%	13.31%	29.16%	62.00%	81.07%

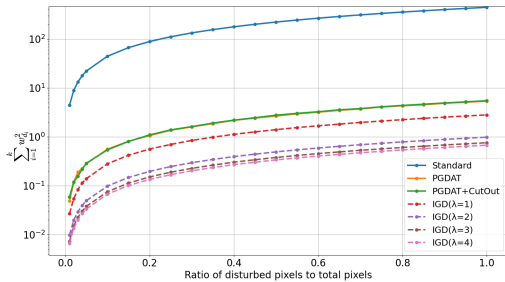


Figure 5: Average $\sum_{i=1}^k w_{d_i}^2$ across different methods on Imagenet-100. Models are attacked by RN.

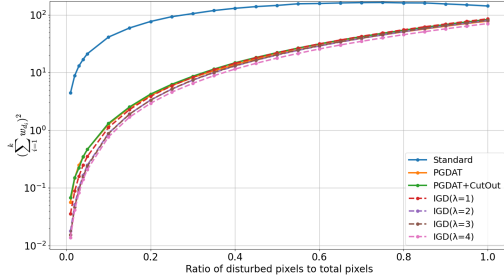


Figure 6: Average $(\sum_{i=1}^k w_{d_i})^2$ across different methods on Imagenet-100. Models are attacked by RN.

in each iteration, which ensures a monotonic descent in the Gini value(see subsection A.9). After increasing $|w_a|$ and decreasing $|w_b|$ by Δ , we obtain new set of w' and have:

$$\sum_{i=1}^k w_{d_i}'^2 = \sum_{i=1}^k w_{d_i}^2 + 2 * \Delta * (\Delta - |w_b| + |w_a|) \leq \sum_{i=1}^k w_{d_i}^2 - 2 * \Delta^2 < \sum_{i=1}^k w_{d_i}^2$$

Consequently, when $\|\vec{w} * \vec{m}\|_1$ is fixed, decreasing $Gini(\vec{w} * \vec{m})$ means decreasing y_σ 's standard deviation. For a more complicated non-linear model like CNN, we can approximate it as a linear score model by computing first-order Taylor expansion: $f^y(x) \approx \vec{w}^T \vec{x} + b$, where our proof may still hold.

As for the multiplicative-additive noise, we can transform it into: $x' = x + (\delta - x) * m$. Formally, given that $x \sim \mathcal{D}(\mu_x, \sigma_x^2)$, we have $y' = y + y_\delta + y_{-x}$ and $E\{(y' - y)^2\} = (\mu_\delta - \mu_x)^2 (\sum_{i=1}^k w_{d_i})^2 + (\sigma_\delta^2 + \sigma_x^2) \sum_{i=1}^k w_{d_i}^2$. Unlike $\sum_{i=1}^k w_{d_i}^2$, $(\sum_{i=1}^k w_{d_i})^2$ doesn't have the same monotonicity as the Gini value. After increasing $|w_a|$ and decreasing $|w_b|$ by Δ , $(\sum_{i=1}^k w_{d_i})^2$ will vary if w_a and w_b have different sign. Consequently, we can only analyze $(\sum_{i=1}^k w_{d_i})^2$ through statistics.

To further validate our thoughts, on Imagenet-100, we measure $\sum_{i=1}^k w_{d_i}^2$ and $(\sum_{i=1}^k w_{d_i})^2$ of models attacked by RN with different number k of perturbed pixels, where $d_i = randomChoice(1...n)$, $d_i \neq d_j (i \neq j)$, and $d_i < d_{i+1}$. Multiple sampling and averaging are conducted to reduce randomness. In Figure 6, the difference in $(\sum_{i=1}^k w_{d_i})^2$ between PGDAT-trained and IGD-trained model is not significant, indicating that when the model is attacked by the multiplicative-additive random noise, the $(\sum_{i=1}^k w_{d_i})^2$ is not the main factor varying robustness of different models. In Figure 5, we observe that all IGD-trained models have lower $\sum_{i=1}^k w_{d_i}^2$ than the PGDAT-trained model. This is consistent with IGD-trained model's better robustness to noise and our proof above. We also measure $\sum_{i=1}^k w_{d_i}^2$ and $(\sum_{i=1}^k w_{d_i})^2$ of models attacked by INA(see subsection A.4) and on other datasets(see subsection A.5).

Also, we find the standard-trained model has larger $\sum_{i=1}^k w_{d_i}^2$ under all number of attacked pixels. However, results in Figure 3 shows that the standard-trained model has better robustness to noise than the PGDAT-trained model. We think this is because the standard-trained model correctly classifies clean samples with high confidence(see Table 4). Even though the standard-trained model's class score is affected by noises with large deviations, the clean sample's class score is large enough to submerge the noise, allowing the standard-trained model to correctly classify the noisy sample. This also boosts IGD-trained models' robustness, as IGD can slightly promote confidence compared to the PGDAT. On Imagenet-C, however, the smaller σ_δ weakens the influence of $\sum_{i=1}^k w_{d_i}^2$. Thus, when tested on Imagenet-C, the noise-robustness of the standard-trained model becomes worse than the PGDAT-trained model's, which is shown in Table 5, Table 6, and Table 7.

As for the occlusion, like the multiplicative-additive noise, we have $y' = y + y_\delta + y_{-x}$. However, unlike the other two types of noise, the occlusion has $\sigma_\delta = 0$, indicating $E\{(y' - y)^2\} = (\mu_\delta - \mu_x)^2 (\sum_{i=1}^k w_{d_i})^2 + \sigma_x^2 \sum_{i=1}^k w_{d_i}^2$. As mentioned in subsection 4.1, pixels that are considered important by the IGD-trained model tend to cluster when λ is not high. This may result in high

$(\sum_{i=1}^k w_{d_i})^2$ (see $\text{IGD}(\lambda=1)$ in Table 4) and worse or non-improved robustness to occlusion, which is shown in Table 3. Moreover, the smaller coefficient of $\sum_{i=1}^k w_{d_i}^2$ weakens the robustness gained by the equal decision pattern, which explains why IOA-robustness gained by IGD is not as notable as the noise-robustness. When λ is increased and regional inequality starts releasing, the relatively low $(\sum_{i=1}^k w_{d_i})^2$ and $\sum_{i=1}^k w_{d_i}^2$ weaken the effect of occlusion, and the IGD-trained models’ robustness to all three types of occlusion are improved.

To conclude, the IGD-trained model and the standard-trained model gain robustness to i.i.d. noise and occlusion because of their equal decision patterns’ suppressing the deviation of class score, and the higher correct classification confidence further boosts their robustness.

5.2 Conjecture on low-resolution dataset

On low-resolution datasets like CIFAR100, though the standard-trained model has a more equal decision pattern, it does not have better robustness to i.i.d. noise and occlusion. Apart from the small gap of $\text{Gini}(A^f(x))$ (see subsection A.7), we hypothesize that more pixels means the equality of the decision pattern being more important. In subsection 5.1, we prove that the Gini value has the same monotonicity as the deviation of the class score. After changing $|w_a|$ and $|w_b|$ by δ , we have $\frac{\Delta \sum_{i=1}^k w_{d_i}^2}{\Delta \text{Gini}(\bar{w} * \bar{m})} = \frac{(\delta - |w_b| + |w_a|) * \sum_{i=1}^k |w_{d_i}|}{a-b} * k$, which indicates when the gap of Gini value is fixed, a larger k means a larger descent on the deviation of the class score and greater importance of the equality of decision pattern. In Figure 3(c), when k is low and $\lambda=2$, the IGD-trained model has lower error rates than the standard-trained. However, as k grows, the standard-trained model tend to have better RN-robustness compared to the IGD-trained model. This may indicates that the importance of the equal decision pattern grows as the number of pixels grows.

Additionally, we acknowledge that the equality of decision pattern and classification confidence are not the only two factors that have influences on the model’s noise- and occlusion-robustness. In Table 4, though PGDAT-trained model with CutOut has larger $\sum_{i=1}^k w_{d_i}^2$ and $(\sum_{i=1}^k w_{d_i})^2$, and has higher error rate on IOA-G and IOA-W, its error rates on IOA-B is much lower than $\text{IGD}(\lambda=1, 2)$, which suggests that there are other factors, like the frequency of perturbation[20], that influence model’s noise- and occlusion-robustness. These factors may overwhelm the equality of decision pattern and classification confidence when the dataset’s resolution is low. To validate our conjecture, we do additional experiments on TinyImaganet[17], which contains images with resolution $64*64$. Results are shown in subsection A.1 and subsection A.5. We can find that improvement of INA-robustness gained by IGD on TinyImagenet is more notable than that on CIFAR100. This may indicates that vulnerability caused by the unequal decision pattern is more notable on high-resolution datasets than on low-resolution datasets.

6 Conclusion

In this paper, we propose a simple yet effective method, called Input Gradient Distillation(IGD), to release the inequality phenomena in l_∞ -adversarial training and to promote l_∞ -adversarially trained model’s robustness to INA, RN, and IOA. By aligning the input gradients of the model being l_∞ -adversarially trained and the fixed standard-trained model, IGD can make l_∞ -adversarially trained model’s decision pattern equal while preserving the model’s adversarial robustness as much as possible. IGD can improve the l_∞ -adversarially trained model’s robustness to i.i.d. noise and occlusion, and such improved robustness has better generalization compared to robustness gained by CutOut. We also formally explain how IGD- and standard-trained model gain robustness to noise and occlusion and claim that the equal decision pattern promotes the model’s robustness by suppressing the deviation of the class score. Also, we find the unsatisfactory performance of IGD on low-resolution datasets and attribute it to the small scale of pixels and the presence of other factors. We hope that this work can inspire future research to alleviate the issue of clustering important pixels and provide a better explanation of how the equality of decision pattern interacts with other factors.

References

- [1] C. Szegedy, W. Zaremba, I. Sutskever, J. Bruna, D. Erhan, I. Goodfellow, and R. Fergus. Intriguing properties of neural networks. *Computer Science*, 2013.

- [2] Aleksander Madry, Aleksandar Makelov, Ludwig Schmidt, Dimitris Tsipras, and Adrian Vladu. Towards deep learning models resistant to adversarial attacks. *arXiv preprint arXiv:1706.06083*, 2017.
- [3] Yisen Wang, Difan Zou, Jinfeng Yi, James Bailey, Xingjun Ma, and Quanquan Gu. Improving adversarial robustness requires revisiting misclassified examples. In *International Conference on Learning Representations*, 2020.
- [4] Yao Qin, Nicholas Frosst, Sara Sabour, Colin Raffel, Garrison Cottrell, and Geoffrey Hinton. Detecting and diagnosing adversarial images with class-conditional capsule reconstructions. *arXiv preprint arXiv:1907.02957*, 2019.
- [5] Shasha Li, Shitong Zhu, Sudipta Paul, Amit Roy-Chowdhury, Chengyu Song, Srikanth Krishnamurthy, Ananthram Swami, and Kevin S Chan. Connecting the dots: Detecting adversarial perturbations using context inconsistency. In *Computer Vision—ECCV 2020: 16th European Conference, Glasgow, UK, August 23–28, 2020, Proceedings, Part XXIII 16*, pages 396–413. Springer, 2020.
- [6] P. Chalasani, Jiefeng Chen, Amrita Roy Chowdhury, S. Jha, and X. Wu. Concise explanations of neural networks using adversarial training. 2018.
- [7] M. Sundararajan, A. Taly, and Q. Yan. Axiomatic attribution for deep networks. 2017.
- [8] Ranjie Duan, YueFeng Chen, Yao Zhu, Xiaojun Jia, Rong Zhang, et al. Inequality phenomenon in l_∞ -adversarial training, and its unrealized threats. In *The Eleventh International Conference on Learning Representations*.
- [9] Robert Dorfman. A formula for the gini coefficient. *The review of economics and statistics*, pages 146–149, 1979.
- [10] Dan Hendrycks and Thomas Dietterich. Benchmarking neural network robustness to common corruptions and perturbations, 2019.
- [11] Andrew Ross and Finale Doshi-Velez. Improving the adversarial robustness and interpretability of deep neural networks by regularizing their input gradients. In *Proceedings of the AAAI Conference on Artificial Intelligence*, volume 32, 2018.
- [12] Chris Finlay and Adam M Oberman. Scaleable input gradient regularization for adversarial robustness. *arXiv preprint arXiv:1905.11468*, 2019.
- [13] Alvin Chan, Yi Tay, and Yew-Soon Ong. What it thinks is important is important: Robustness transfers through input gradients. In *Proceedings of the IEEE/CVF Conference on Computer Vision and Pattern Recognition (CVPR)*, June 2020.
- [14] Rulin Shao, Jinfeng Yi, Pin-Yu Chen, and Cho-Jui Hsieh. How and when adversarial robustness transfers in knowledge distillation?, 2021.
- [15] Maksym Andriushchenko and Nicolas Flammarion. Understanding and improving fast adversarial training. *CoRR*, abs/2007.02617, 2020. URL <https://arxiv.org/abs/2007.02617>.
- [16] Alex Krizhevsky, Geoffrey Hinton, et al. Learning multiple layers of features from tiny images. 2009.
- [17] Jia Deng, Wei Dong, Richard Socher, Li-Jia Li, Kai Li, and Li Fei-Fei. Imagenet: A large-scale hierarchical image database. In *2009 IEEE conference on computer vision and pattern recognition*, pages 248–255. Ieee, 2009.
- [18] Kaiming He, Xiangyu Zhang, Shaoqing Ren, and Jian Sun. Deep residual learning for image recognition. In *2016 IEEE Conference on Computer Vision and Pattern Recognition (CVPR)*, pages 770–778, 2016. doi: 10.1109/CVPR.2016.90.
- [19] Karen Simonyan, Andrea Vedaldi, and Andrew Zisserman. Deep inside convolutional networks: Visualising image classification models and saliency maps, 2014.

- [20] Dong Yin, Raphael Gontijo Lopes, Jonathon Shlens, Ekin D. Cubuk, and Justin Gilmer. A fourier perspective on model robustness in computer vision, 2020.
- [21] Rahul Rade and Seyed-Mohsen Moosavi-Dezfooli. Reducing excessive margin to achieve a better accuracy vs. robustness trade-off. In *International Conference on Learning Representations*, 2022. URL <https://openreview.net/forum?id=Azh9QBQ4tR7>.
- [22] Avanti Shrikumar, Peyton Greenside, Anna Shcherbina, and Anshul Kundaje. Not just a black box: Learning important features through propagating activation differences. *CoRR*, abs/1605.01713, 2016. URL <http://arxiv.org/abs/1605.01713>.
- [23] Scott M. Lundberg and Su-In Lee. A unified approach to interpreting model predictions. *CoRR*, abs/1705.07874, 2017. URL <http://arxiv.org/abs/1705.07874>.
- [24] Daniel Smilkov, Nikhil Thorat, Been Kim, Fernanda Viégas, and Martin Wattenberg. Smooth-Grad: removing noise by adding noise. *arXiv e-prints*, art. arXiv:1706.03825, June 2017. doi: 10.48550/arXiv.1706.03825.
- [25] Narine Kokhlikyan, Vivek Miglani, Miguel Martin, Edward Wang, Bilal Alsallakh, Jonathan Reynolds, Alexander Melnikov, Natalia Kliushkina, Carlos Araya, Siqi Yan, and Orion Reblitz-Richardson. Captum: A unified and generic model interpretability library for pytorch, 2020.
- [26] Francesco Croce and Matthias Hein. Reliable evaluation of adversarial robustness with an ensemble of diverse parameter-free attacks. *CoRR*, abs/2003.01690, 2020. URL <https://arxiv.org/abs/2003.01690>.
- [27] Logan Engstrom, Andrew Ilyas, Hadi Salman, Shibani Santurkar, and Dimitris Tsipras. Robustness (python library), 2019. URL <https://github.com/MadryLab/robustness>.

A Appendix

A.1 Results on TinyImagenet

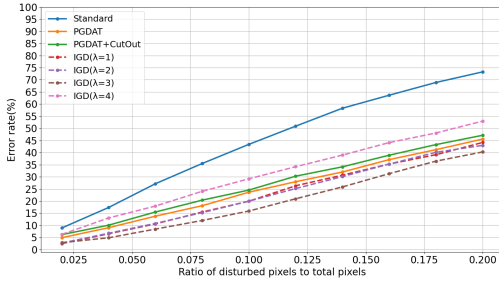


Figure 7: Error rate \downarrow of Resnet18 trained with different methods on TinyImagenet. Model is attacked by INA1 with saliency map.

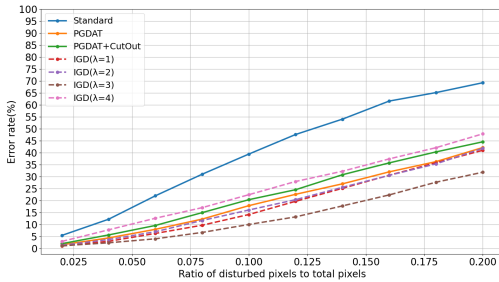


Figure 8: Error rate \downarrow of Resnet18 trained with different methods on TinyImagenet. Model is attacked by INA2 with saliency map.

We post error rates of Resnet18 attacked by INA nad RN on TinyImagenet. We also report Average confidence, $Gini(A^f(x))$, and $\left\| \frac{\partial f^y(x)}{\partial x} \right\|_1$ of Resnet18 across different methods on TinyImagenet.

A.2 Experiment setting

A.2.1 Datasets, models and attribution methods

We perform our experiment on CIFAR100[16] and Imagenet-100[17](same setting as [21]) for lower computation complexity. We use Resnet18[18] for both CIFAR100 and Imagenet-100. We use Input X Gradients[22], Integrated Gradients[7], Shapley Value[23], SmoothGrad[24], and Saliency map[19], which are provided by Kohlikyan et al. [25].

A.2.2 Training setup

For fairness, all of the models are trained for 150 Epochs by SGD with momentum 0.9 and weight decay $5e-4$. The initial learning rate is 0.1 and is reduced on the plateau with factor 0.1. All adversarial examples used during the training phase are generated by PGD[2] with $\epsilon = 8/255$, $stepsize = 2/255$, and $iter = 10$. We choose the standard-trained model with the best standard accuracy and the l_∞ -adversarially- or IGD-trained model with the best PGD-10 accuracy for evaluation.

A.2.3 Evaluation setup

To evaluate the adversarial robustness of trained models fairly, we use AutoAttack[26] with $\epsilon = 8/255$. We use error rate to evaluate models' robustness to attacks introduced in subsection 2.4 and on noisy images of Imagenet-C[10] where we select classes in Imagenet-100. When we compare the robustness of different models, the error rate is the proportion of misclassified samples among samples correctly classified by all models being compared. We follow the settings of the attack algorithm in [8] and

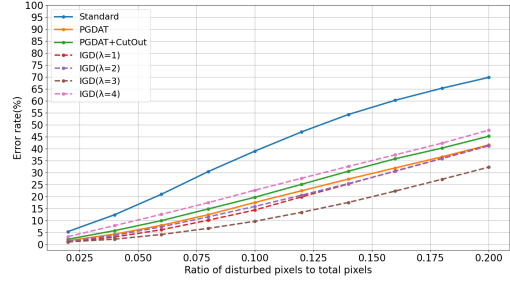


Figure 9: Error rate \downarrow of Resnet18 trained with different methods on TinyImagenet. Model is attacked by RN.

Table 8: Average confidence, $Gini(A^f(x))$, and $\left\| \frac{\partial f^y(x)}{\partial x} \right\|_1$ of Resnet18 across different methods on TinyImagenet.

Method	Metric	Confidence	$Gini(A^f(x))$	$\ A^f(x)\ _1$
Standard		89.24%	0.501	6832932
PGDAT[2]		51.65%	0.578	439303
PGDAT+CutOut[8]		47.85%	0.585	411621
IGD($\lambda=1$)		51.87%	0.565	445603
IGD($\lambda=2$)		50.96%	0.558	463296
IGD($\lambda=3$)		47.97%	0.549	473268
IGD($\lambda=4$)		40.58%	0.536	432738

will clarify attack parameters if necessary. When using IOA, we set $N=10$ and $R=4$ for CIFAR100 and set $R=20$ for Imagenet-100. We mainly use Saliency Map[19] to generate attribution maps and will note if other attribution methods are used. When measuring regional inequality, we set $r = 16$ for Imagenet-100 and $r = 4$ for CIFAR100.

A.3 Failure case on CIFAR10

IGD is designed to align the attribution vector’s direction rather than to alter the norm of the attribution vector significantly. In most cases, like on Imagenet-100, CIFAR100, and TinyImagenet, IGD does well. On CIFAR10, however, we find that IGD alters the norm of the attribution vector compared to other cases and may worsen the model’s robustness.

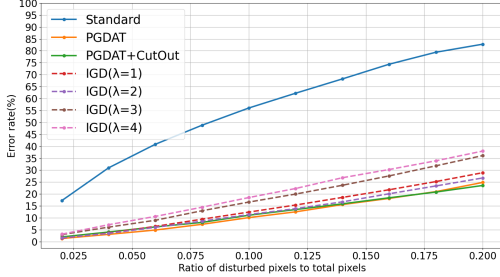


Figure 10: Error rate↓ of Resnet18 trained with different methods on CIFAR10. Model is attacked by INA1.

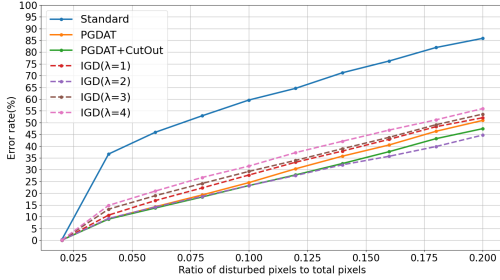


Figure 11: Error rate↓ of Resnet18 trained with different methods on CIFAR10. Model is attacked by INA2.

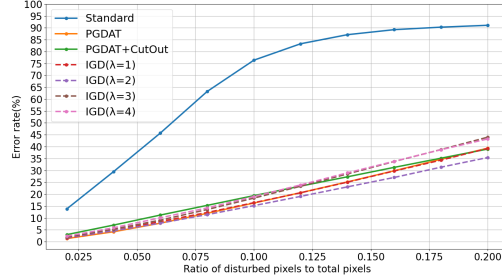


Figure 12: Error rate↓ of Resnet18 trained with different methods on CIFAR10. Model is attacked by RN.

Table 9: $\left\| \frac{\partial f^y(x)}{\partial x} \right\|_1$ of Resnet18 across methods on CIFAR10.

Dataset	Method	$\left\ \frac{\partial f^y(x)}{\partial x} \right\ _1$
CIFAR10	Standard	12175720(100%)
	PGDAT [2]	591025(4.85%)
	PGDAT+CutOut [8]	555282(4.56%)
	IGD($\lambda=1$)	428836(3.52%)
	IGD($\lambda=2$)	308085(2.53%)
	IGD($\lambda=3$)	258002(2.12%)
	IGD($\lambda=4$)	254231(2.09%)

A.4 $\sum_{i=1}^k w_{d_i}^2$ and $(\sum_{i=1}^k w_{d_i})^2$ under INA on Imagenet-100

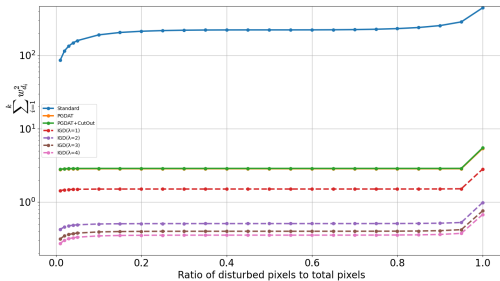


Figure 13: Average $\sum_{i=1}^k w_{d_i}^2$ across different methods on Imagenet-100 attacked by INA.

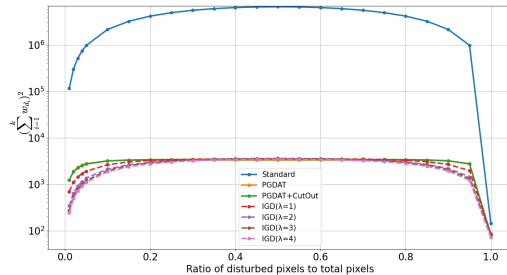


Figure 14: Average $(\sum_{i=1}^k w_{d_i})^2$ across different methods on Imagenet-100 attacked by INA.

On Imagenet-100, we also measure $\sum_{i=1}^k w_{d_i}^2$ and $(\sum_{i=1}^k w_{d_i})^2$ of models attacked by INA using saliency map as guidance(see Figure 13 and Figure 14). Because INA chooses pixels with high

attribution (gradient) value, both $\sum_{i=1}^k w_{d_i}^2$ and $(\sum_{i=1}^k w_{d_i})^2$ of the PGDAT-trained model rise faster than that of IGD-trained models, which results in PGDAT-trained model’s worse INA-robustness.

A.5 $\sum_{i=1}^k w_{d_i}^2$ and $(\sum_{i=1}^k w_{d_i})^2$ under RN on CIFAR100 and TinyImagenet

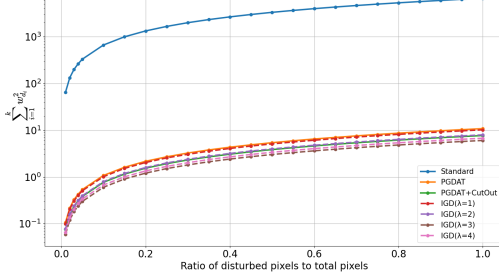


Figure 15: Average $\sum_{i=1}^k w_{d_i}^2$ across different methods on CIFAR100 attacked by RN.

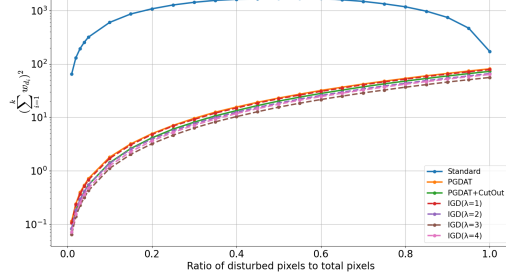


Figure 16: Average $(\sum_{i=1}^k w_{d_i})^2$ across different methods on CIFAR100 attacked by RN.

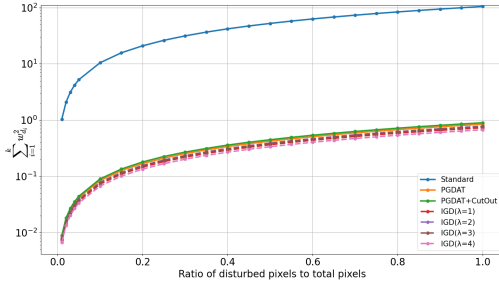


Figure 17: Average $\sum_{i=1}^k w_{d_i}^2$ across different methods on TinyImagenet attacked by RN.

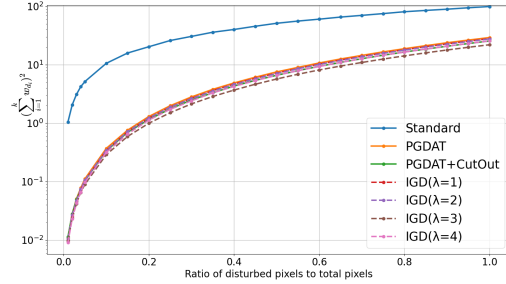


Figure 18: Average $(\sum_{i=1}^k w_{d_i})^2$ across different methods on TinyImagenet attacked by RN.

We also measure $\sum_{i=1}^k w_{d_i}^2$ and $(\sum_{i=1}^k w_{d_i})^2$ under RN on CIFAR100 and TinyImagenet. Results are shown in Figure 15, Figure 16, Figure 17, and Figure 18.

A.6 How to choose λ for IGD

In subsection 4.1, we show that on Imagenet-100, within a specific interval of λ , the descent of $Gini(A^f(x))$ and error rate to INA and RN is huge, and the adversarial robustness does not drop a lot. Thus, if a user wants to promote the model’s INA- and RN- robustness while preserving the adversarial robustness, stop increasing λ when $Gini(A^f(x))$ is no longer rapidly decreasing. If a user wants to promote the model’s IOA-robustness, choose the λ when $Gini(A_r^f(x))$ stops decreasing or the adversarial robustness is below the user’s tolerance. Specifically, we suggest user try $\lambda = 2$ on datasets with the similar resolution as Imagenet-100.

A.7 The small gap of $Gini(A^f(x))$ on low-resolution datasets

Some may question whether the small gap of $Gini(A^f(x))$ between the standard- and l_∞ -adversarially trained model is common on low resolution datasets and will it be influenced by the number of classes? To answer these, we evaluate $Gini(A^f(x))$ and $Gini(A_r^f(x))$ of Resnet50 trained on CIFAR10 provided by Engstrom et al. [27] and Resnet18 trained on TinyImagenet[17] and CIFAR100[16] by us. Results are shown in Table 10. On CIFAR10, CIFAR100, and TinyImagenet, the difference of $Gini(A^f(x))$ between standard-trained and l_∞ -adversarially trained model is still much smaller than that on Imagenet-100(see Table 1 and Table 11). This may indicate that the small gap of $Gini(A^f(x))$ between the standard-trained model and the l_∞ -adversarially trained model is common. Also, we find that the gap of $Gini(A_r^f(x))$ in Table 10 is as large as that on Imagenet-100. We believe that on higher resolution datasets like Imagenet-100, it’s the inequality

within the region that further expands the gap of $Gini(A^f(x))$ and the downsample operation of calculating $Gini(A_r^f(x))$ cover up such inequality. Thus, we think that it's the downsample operation, which is usually used in building up low-resolution datasets like CIFAR, that reduces the gap of $Gini(A^f(x))$.

Table 10: Global Gini value and regional Gini value of standard-trained and l_∞ -adversarially trained model on CIFAR10 and TinyImagenet. r is set to 4 on CIFAR10 and CIFAR100, and is set to 8 on TinyImagenet.

Dataset	Metric	Method		Integrated Gradients	Input X Gradients	GradShap	SmoothGrad	Saliency Map
		Model						
CIFAR10	$Gini(A^f(x))$	Std. trained		0.615	0.616	0.613	0.593	0.532
		Adv. trained		0.719	0.745	0.734	0.889	0.737
	$Gini(A_r^f(x))$	Std. trained		0.346	0.426	0.424	0.518	0.337
		Adv. trained		0.477	0.596	0.595	0.778	0.592
CIFAR100	$Gini(A^f(x))$	Std. trained		0.611	0.581	0.587	0.388	0.530
		Adv. trained		0.672	0.702	0.696	0.640	0.666
	$Gini(A_r^f(x))$	Std. trained		0.304	0.412	0.424	0.320	0.342
		Adv. trained		0.377	0.569	0.584	0.554	0.527
TinyImagenet	$Gini(A^f(x))$	Std. trained		0.609	0.575	0.586	0.452	0.501
		Adv. trained		0.650	0.653	0.673	0.674	0.578
	$Gini(A_r^f(x))$	Std. trained		0.235	0.348	0.365	0.345	0.273
		Adv. trained		0.333	0.461	0.499	0.552	0.396

A.8 IGD's training time

Theoretically, compared to PGDAT, IGD only needs extra cost to obtain the standard-trained model's input gradient. The input gradient of the model being l_∞ -adversarially trained can be obtained by the first iteration of the adversarial attack, like PGD. Given that we run k attack's iterations for each batch and the standard-trained model has the same scale as the model being trained, the total time expense increases by above $\frac{k+1}{k}$ for the second-order derivative may have extra cost. In our implementation, we do not make use of the first iteration to get the clean sample's gradient for low coupling. On Imagenet-100, using NVIDIA A100 40GB, PGDAT takes 13 minutes for an epoch, and IGD takes 18 minutes for an epoch. Both PGDAT and IGD use PGD-10 to generate adversarial examples.

A.9 How to decrease Gini value monotonically

For conciseness, let's assume that $\forall i \in n, w_i \geq 0$ and $w_i \leq w_{i+1}$, because when calculating the Gini value, we usually take the absolute value of w . First, if we do not change two elements ($w_a < w_b$ and $a < b$) positions and we decrease the bigger one by δ while increasing the smaller one by δ , the Gini value is decreased. Saying we have a new population w' , this can be proved because $\sum_{i=1}^n (n+1-i) * w'_i = \sum_{i=1}^n (n+1-i) * w_i + (n+1-a) * \Delta - (n+1-b) * \Delta > \sum_{i=1}^n (n+1-i) * w_i$. Thus, this results in Equation 2's descent.

Next, we prove that the operation, where we select two elements ($w_a < w_b$), increase w_a by Δ , and decrease w_b by Δ , which somehow change w_a and w_b 's position, can be decomposed into a sequence of operations that do not change elements' relative positions.

Saying after all operations, w_a and w_b becomes $w_{a'}$ and $w_{b'}$ ($a \leq a' \leq b' \leq b$). In each operation, we try to decrease w_b by $w_{a+1} - w_a$, and add it to w_a . This operation will have two results. One is we successfully perform this operation without changing any element's position, which decreases the Gini value, and the next operation between w_a and w_b is the same as the operation between w_{a+1} and w_b . The other is that decreasing w_b will result in w_b 's being smaller than w_{b-1} . Under this condition, we decrease w_b by $w_b - w_{b-1}$, and add it to w_a , which also decrease Gini value. In this case, the next operation between w_a and w_b is the same as the operation between w_a and w_{b-1} .

Thus, we can decompose any operation of changing two elements' values into a sequence of operations mentioned above, and ensure that each operation in the sequence will decrease the Gini value, which proves that the operation of selecting two elements ($w_a < w_b$) and reducing the difference between them will decrease Gini value. We can also prove that by decreasing w_a by Δ , and by increasing w_b by Δ , we can increase the Gini value monotonically, which is symmetric to the proof above.

A.10 $Gini(A^f(x))$ and $Gini(A_r^f(x))$ using other attribution method

Table 11: Global Gini value and regional Gini value across different datasets, training methods, and attribution methods.

Dataset	Attr. method	Integrated Gradients		Input X Gradient		GradShap		SmoothGrad	
		$Gini(A^f(x))$	$Gini(A_r^f(x))$	$Gini(A^f(x))$	$Gini(A_r^f(x))$	$Gini(A^f(x))$	$Gini(A_r^f(x))$	$Gini(A^f(x))$	$Gini(A_r^f(x))$
CIFAR100	Standard	0.611	0.304	0.581	0.412	0.587	0.424	0.388	0.320
	PGDAT [2]	0.672	0.377	0.702	0.569	0.696	0.584	0.640	0.554
	PGDAT+CutOut [8]	0.673	0.343	0.701	0.568	0.693	0.580	0.605	0.508
	IGD($\lambda=1$)	0.676	0.381	0.697	0.565	0.698	0.588	0.639	0.559
	IGD($\lambda=2$)	0.655	0.367	0.677	0.551	0.674	0.568	0.617	0.543
	IGD($\lambda=3$)	0.642	0.362	0.660	0.534	0.660	0.557	0.607	0.542
	IGD($\lambda=4$)	0.636	0.361	0.648	0.523	0.650	0.548	0.607	0.543
Imagenet-100	Standard	0.633	0.285	0.605	0.407	0.610	0.413	0.564	0.502
	PGDAT [2]	0.936	0.382	0.942	0.601	0.947	0.633	0.941	0.594
	PGDAT+CutOut [8]	0.923	0.350	0.935	0.596	0.941	0.624	0.933	0.562
	IGD($\lambda=1$)	0.829	0.399	0.854	0.592	0.865	0.627	0.915	0.696
	IGD($\lambda=2$)	0.739	0.395	0.772	0.589	0.791	0.625	0.815	0.698
	IGD($\lambda=3$)	0.715	0.375	0.744	0.573	0.764	0.609	0.807	0.692
	IGD($\lambda=4$)	0.701	0.365	0.735	0.571	0.754	0.606	0.796	0.700

See Table 11.

A.11 Error rate of INA using other attribution methods

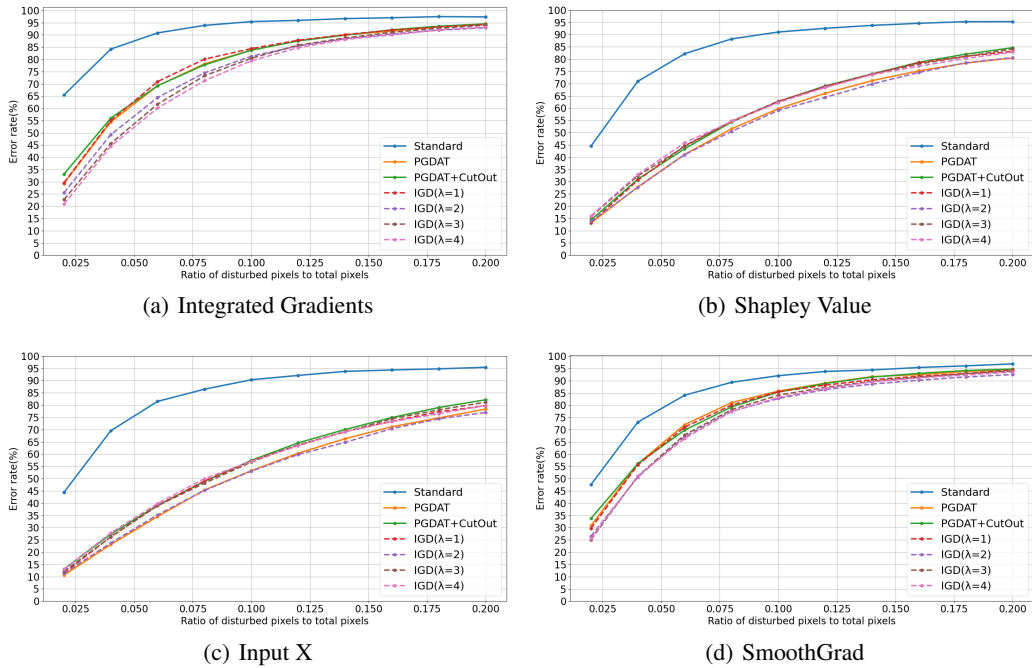


Figure 19: Error rate of models trained with different methods on CIFAR100 attacked by INA1.

We post error rates of models attacked by INA with attribution methods other than saliency map, where our findings in subsection 4.2 still hold. Results are shown in Figure 19, Figure 20, Figure 21, and Figure 22.

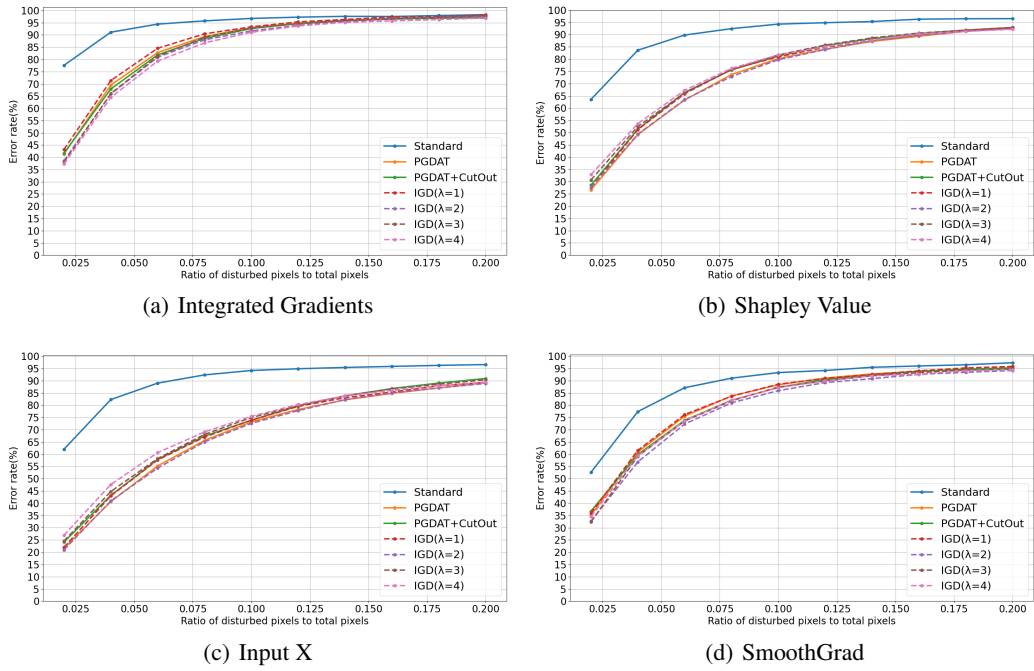


Figure 20: Error rate↓ of models trained with different methods on CIFAR100 attacked by INA2.

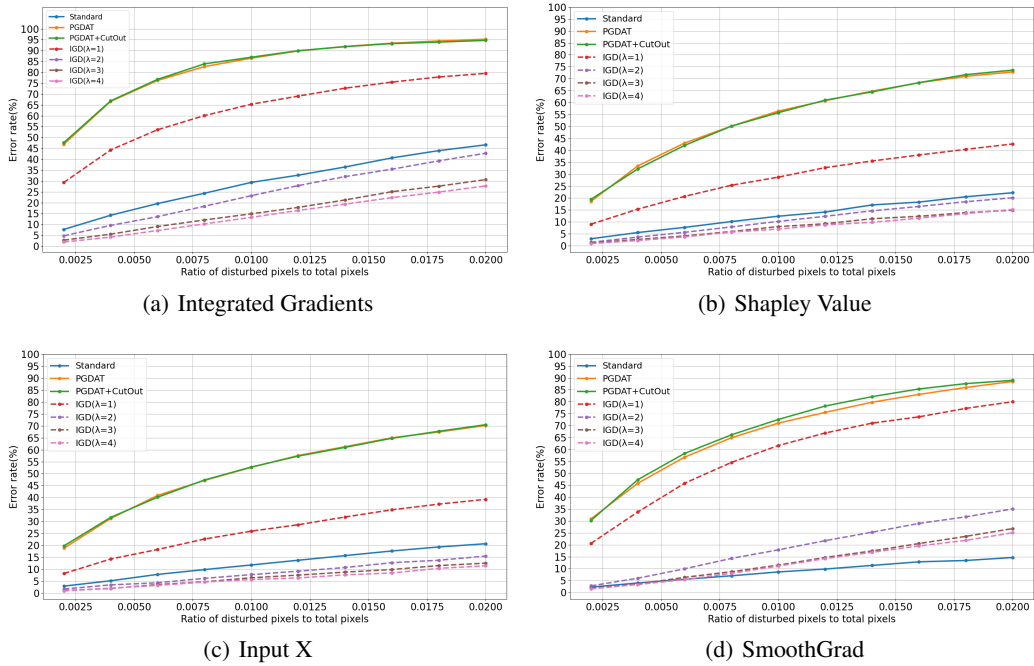
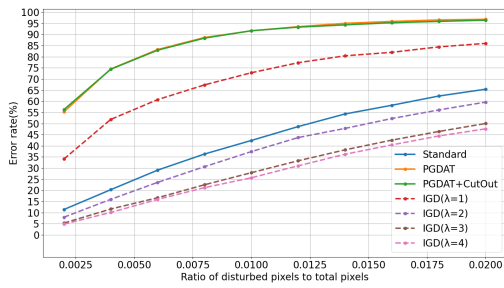
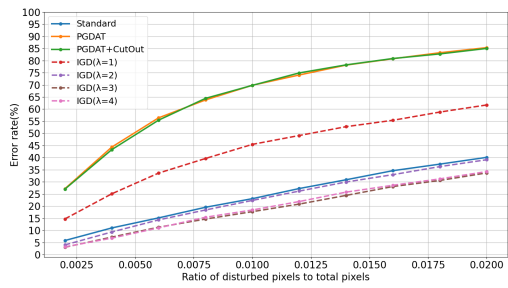


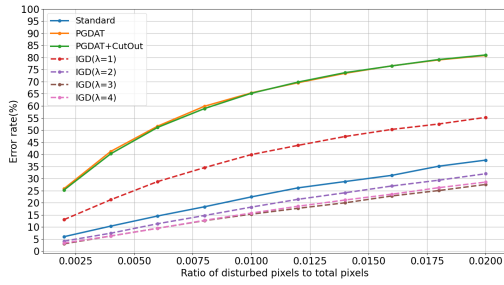
Figure 21: Error rate↓ of models trained with different methods on Imagenet-100 attacked by INA1.



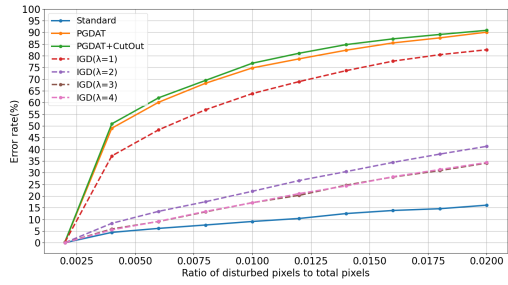
(a) Integrated Gradients



(b) Shapley Value



(c) Input X



(d) SmoothGrad

Figure 22: Error rate \downarrow of models trained with different methods on Imagenet-100 attacked by INA2.

A.12 Error rate of IOA using other attribution methods

Table 12: Error rate \downarrow of models across different methods, datasets, and types of IOA (N=10, R=4 for CIFAR100 and R=20 for Imagenet-100). Attribution maps are generated by Integrated Gradients.

Dataset	Method Attack	IOA-B	IOA-G	IOA-W
CIFAR100	Standard	72.51%	48.03%	62.77%
	PGDAT [2]	59.02%	37.08%	56.51%
	PGDAT+CutOut [8]	16.90%	34.66%	56.55%
	IGD($\lambda=1$)	57.08%	35.80%	57.53%
	IGD($\lambda=2$)	56.74%	35.28%	55.03%
	IGD($\lambda=3$)	57.74%	35.02%	52.04%
	IGD($\lambda=4$)	60.80%	34.95%	53.54%
Imagenet-100	Standard	29.13%	13.84%	23.27%
	PGDAT [2]	43.49%	14.89%	47.93%
	PGDAT+CutOut [8]	31.07%	14.53%	47.73%
	IGD($\lambda=1$)	38.86%	17.03%	45.10%
	IGD($\lambda=2$)	34.88%	11.97%	36.42%
	IGD($\lambda=3$)	35.24%	10.78%	32.48%
	IGD($\lambda=4$)	31.92%	11.14%	33.53%

Table 13: Error rate \downarrow of models across different methods, datasets, and types of IOA (N=10, R=4 for CIFAR100 and R=20 for Imagenet-100). Attribution maps are generated by Shapley Value.

Dataset	Method Attack	IOA-B	IOA-G	IOA-W
CIFAR100	Standard	61.59%	34.57%	44.52%
	PGDAT [2]	37.99%	16.93%	30.77%
	PGDAT+CutOut [8]	12.37%	18.45%	30.22%
	IGD($\lambda=1$)	35.54%	16.38%	31.03%
	IGD($\lambda=2$)	34.12%	15.27%	29.91%
	IGD($\lambda=3$)	34.73%	16.74%	29.27%
	IGD($\lambda=4$)	36.35%	16.14%	28.40%
Imagenet-100	Standard	20.32%	7.59%	13.48%
	PGDAT [2]	27.65%	10.65%	36.09%
	PGDAT+CutOut [8]	20.45%	10.45%	36.49%
	IGD($\lambda=1$)	29.32%	10.12%	34.58%
	IGD($\lambda=2$)	20.02%	6.18%	24.98%
	IGD($\lambda=3$)	17.72%	5.39%	22.65%
	IGD($\lambda=4$)	16.50%	5.75%	21.60%

Table 14: Error rate \downarrow of models across different methods, datasets, and types of IOA (N=10, R=4 for CIFAR100 and R=20 for Imagenet-100). Attribution maps are generated by Input X.

Dataset	Method Attack	IOA-B	IOA-G	IOA-W
CIFAR100	Standard	59.92%	32.41%	42.33%
	PGDAT [2]	40.88%	18.78%	36.70%
	PGDAT+CutOut [8]	12.68%	18.23%	35.54%
	IGD($\lambda=1$)	38.60%	17.07%	37.13%
	IGD($\lambda=2$)	37.13%	17.09%	35.42%
	IGD($\lambda=3$)	37.73%	16.81%	35.04%
	IGD($\lambda=4$)	39.79%	17.69%	35.09%
Imagenet-100	Standard	19.00%	6.67%	11.37%
	PGDAT [2]	30.83%	11.18%	38.49%
	PGDAT+CutOut [8]	21.14%	10.65%	37.34%
	IGD($\lambda=1$)	31.03%	10.55%	36.42%
	IGD($\lambda=2$)	21.89%	6.15%	26.66%
	IGD($\lambda=3$)	19.26%	5.59%	23.11%
	IGD($\lambda=4$)	17.42%	5.26%	23.54%

Table 15: Error rate \downarrow of models across different methods, datasets, and types of IOA (N=10, R=4 for CIFAR100 and R=20 for Imagenet-100). Attribution maps are generated by SmoothGrad.

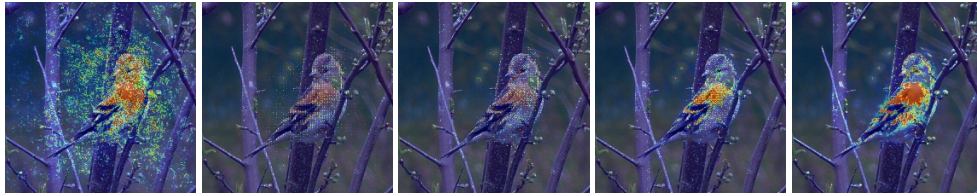
Dataset	Method Attack	IOA-B	IOA-G	IOA-W
CIFAR100	Standard	48.96%	31.46%	47.84%
	PGDAT [2]	37.30%	21.91%	43.28%
	PGDAT+CutOut [8]	11.30%	20.18%	41.69%
	IGD($\lambda=1$)	36.35%	19.16%	41.57%
	IGD($\lambda=2$)	34.07%	18.71%	41.69%
	IGD($\lambda=3$)	36.04%	19.42%	41.64%
	IGD($\lambda=4$)	39.55%	18.92%	40.67%
Imagenet-100	Standard	9.63%	4.83%	8.74%
	PGDAT [2]	21.30%	8.78%	29.62%
	PGDAT+CutOut [8]	15.98%	8.45%	30.54%
	IGD($\lambda=1$)	22.29%	9.70%	30.28%
	IGD($\lambda=2$)	16.21%	5.62%	22.42%
	IGD($\lambda=3$)	14.79%	3.98%	19.00%
	IGD($\lambda=4$)	14.23%	4.24%	18.05%

We post error rates of models attacked by IOA with attribution methods other than saliency map, where our findings in subsection 4.3 still hold. Results are shown in Table 12, Table 13, Table 14, and Table 15.

A.13 More visualization of attribution maps



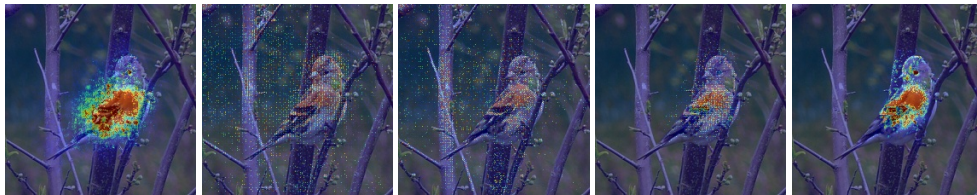
(a) IG



(b) GradShap



(c) Input X



(d) SmoothGrad

Figure 23: Visualization of attribution maps of Imagenet-100 across different attribution methods. From left to right: Standard training, PGDAT, PGDAT+CutOut, $IGD(\lambda = 1)$, $IGD(\lambda = 4)$

We post visualizations of other attribution methods in Figure 23, and results don't vary a lot. This indicates that our methods and analysis will not differ significantly due to differences in attribution methods.